Supplementary Information (SI) for Journal of Materials Chemistry C.
This journal is © The Royal Society of Chemistry 2025

Supporting Information

Self-trapped exciton luminescence of Tellurium doped Zero-dimensional Tetraethyl Tin Chloride for Optical Thermometry

Chen Chen [a], Hailong Yu [a], Hongbo Qi [a], Gaoke Dong [a], Jing Li [a], Gang Yang [a], and Wenzhi Wu [a, *]

[a] School of Electronic Engineering, Heilongjiang University, Heilongjiang, 150080, China

corresponding author's Email: wuwenzhi@hlju.edu.cn

Contents

1. Experimental section

1.1 Materials and reagents

The following chemicals were purchased and used without further purification: Ammonia chloride ($C_8H_{20}NCl$, 99.9%, Macklin), tin$^{(IV)}$ chloride pentahydrate ($SnCl_4 \cdot 5H_2O$, 99.995%, Macklin), hydrochloric acid (HCl, AR, 37 wt%, Harbin Polytechnic Chem. Reag. Co. Ltd), Tellurium dioxide ($TeO_2SnCl_4 \cdot 5H_2O$, 99.995%, Macklin) and Isopropyl alcohol (C_3H_8O, AR, 99.5%, Macklin).

1.2 Preparation and growth of $(TEA)_2SnCl_6$: *x*% Te

The hydrothermal method was employed to synthesize NSCs and NSTCs. Initially, 2 mmol of $C_8H_{20}NCl$, (1-*x*) mmol of $SnCl_4 \cdot 5H_2O$, *x* mmol of TeO_2 (where *x*=0, 0.001,0.005, 0.01, 0.05, 0.10, 0.20 mmol), and 6 ml of HCl were sequentially added to a 25 mL polytetrafluoroethylene (PTFE) container. Subsequently, the mixture was sonicated for 10 minutes to ensure complete dissolution. The resulting solution was then transferred to a stainless-steel Parr autoclave and subjected to a reaction at 180 °C for 12 h. Afterward, the solution was cooled down to 30 °C at a rate of 10 °C/h to ensure a stable temperature reduction. Finally, the obtained crystals were washed three times with isopropanol to remove any residual reactants or adsorbed metal ions on the surface. The product was then dried at 60 °C for 24 h to yield the final product.

1.3 Characterization

Single-crystal X-ray diffraction (SCXRD) data is collected using a Bruker AXS diffractometer (equipped with Mo *Kα* radiation). Powder X-ray diffraction (PXRD) analysis is performed on a Panalytical X'PERT Pro Powder X-ray diffractometer (equipped with Cu *Kα* radiation). Simulated powder patterns are calculated by using VESTA software employing Crystallographic Information Files (CIF) from single crystal X-ray experiments. Energy dispersive spectrometry (EDS) is performed using an accessory for a ZEISS G500 scanning electron microscope. Thermogravimetric analysis (TGA) tests are performed using equipment (Perkin Elmer, TGA 400). Differential scanning calorimetry (DSC) measurements are performed using an instrument (STA 499 F5, Netzsch) with a heating rate of 10 K/min.

1.4 Spectral measurements

Steady-state excitation is performed using a 405 nm continuous wave (CW) laser (FN-360-20 mW, CNI laser) as the excitation source. Steady-state photoluminescence (PL) spectra are collected using a spectrometer (HR4000CG-UV-NIR, Ocean Optics). Higher TRPL dynamics were carried out by a time correlated single

photon counting (TCSPC) systems, which included a monochromator equipped with a detector (SPCM-01-20, Holita) and single photon counting electronics module (FLA-130, Holita) accounting for data acquisition. A laser (MDL-PS-405, CNI Laser), with a pulse width of 200 picosecond (ps) at 405 nm, served as the excitation and trigger source. Raman spectroscopy was performed at both room temperature and variable temperatures using a 671 nm laser for excitation. Temperature-dependent PL and Raman measurements were performed using a vacuum liquid-nitrogen cryostat (Cryo-77, Oriental Koji) with a range of 80-480 K and a temperature controller. Temperature-dependent PL measurements are performed using a vacuum liquid nitrogen cryostat (Cryo-77, Oriental Koji). PL emission and excitation spectra are measured by F-4600 fluorescence spectrophotometer.

2. Calculation method

We performed First-principles calculation on the $(TEA)_2SnCl_6$ and $(TEA)_2SnCl_6$: 5%Te structure using the Vienna Ab-initio Simulation Package (VASP) [1]. The crystal structure visualization was presented with the help of VESTA software. During the simulations, the generalized gradient approximation (GGA) of Perdew-Burke-Ernzerhof (PBE) is used to describe the exchange-correlation functional and the choice is made to optimize the cell with an ultrasoft pseudopotential [2, 3]. A 4×2×4 Monk horst Pack grid is set up to simulate the Brillouin zone, where the kinetic cut-off energy is 400 eV and the energy band structure is drawn along the high symmetry K point. The highly symmetrical K points are set to Γ-Z-D-B-Γ-A-E-Z for the calculated electronic energy band structure. The calculation converges the total energy to be lower than 1.0×10^{-5} eV per atom. The Hellmann-Feynman force on each atom was converged to lower than 0.01eV/Å.

Table S1 The result of ICP-OES measurements for (TEA)2SnCl6: x%Te MCs.

Te/Sn molar feed ratio	actual Sn concentration (mg/L)	actual Te concentration (mg/L)	actual Te-to-Sn molar ratio
0.001:0.999	8.2420	5.1840	0.0025%
0.005:0.995	7.9580	5.6900	0.0033%
0.01:0.99	8.4220	9.2970	0.0221%
0.05:0.95	8.5940	0.4748	0.0342%
0.1:0.9	7.9680	1.4520	0.5306%
0.2:0.8	6.2270	2.4450	1.1933%

Table S2 Crystal data and structure refinement for $(TEA)_2SnCl_6$

Compound	$(C_8H_{20}N)_2SnCl_6$
Empirical formula	$C_{16}H_{40}Cl_6N_2Sn$
Formula weight	591.89
Temperature/K	150.00
Crystal system	monoclinic
Space group	C2/c
a/Å	13.9341(5)
b/Å	14.4459(4)
c/Å	12.8883(3)
α/°	90
β/°	91.4280(10)
γ/°	90
Volume/Å^3	2593.49(13)
Z	4
ρ_{calcg}/cm^3	1.516
μ/mm^1	1.608
F(000)	1208.0
Crystal size/mm^3	0.2×0.15×0.1
Radiation	Mo *Kα* (*λ*=0.71073)

2θ range for data collection/°	4.062 to 52.796
Index ranges	$-17\leq h\leq 17$, $-18\leq k\leq 18$, $-15\leq l\leq 16$
Reflections collected	25585
Independent reflections	2667 [R_{int}=0.0325, R_{sigma}=0.0158]
Data/restraints/parameters	2667/0/159
Goodness-of-fit on F^2	1.060
Final $R_{indexes}$ [$I>=2\sigma(I)$]	R_1=0.0209, wR_2=0.0522
Final $R_{indexes}$ [all data]	R_1=0.0277, wR_2 = 0.0550
Largest diff. peak/hole/eÅ^{-3}	0.27/-0.35

Table 3 Comparison of performance parameters with other thermometric materials.

Material	**Method**	S_R **(%K^{-1})**	S_A **(K^{-1})**	**Temperature (K)**	**Refs**
$Ba_2Y_2Ge_4O1_3$: Dy^{3+}, Tm^{3+}	FIR	0.772 (298K)	0.641×10^{-2} (298 K)	298-473	4
Bi_3TeBO_9: Er^{3+}	FIR	1.02 (298K)	0.33 (473 K)	298-473	5
$Na_2Y_2TeB_2O_{10}$: Tb^{3+}	FIR	2.49 (475K)	2.16×10^{-2} (300 K)	300-475	6
Te^{4+}: $Cs_2InCl_5\cdot H_2O$	FL	0.062 (320K)	-	240-380	7
$Ca_{2.6}K_{0.2}La_{0.13}(PO_4)_2$: Dy^{3+}, Eu^{3+}	FIR	0.181 (300K)	2.06×10^{-3} (300 K)	303-543	8
SLLT: Eu^{3+}, Mn^{4+}	FIR	0.33 (340K)	-	80-500	9
$CaBa_2WO_6$: Er^{3+}, Mg^{2+}	FIR	0.009 (386K)	-	298-575	10
Te^{4+}: TEA_2SnCl_6	FL	0.57 (100K)	1×10^{-2} (120 K)	100-340	This work

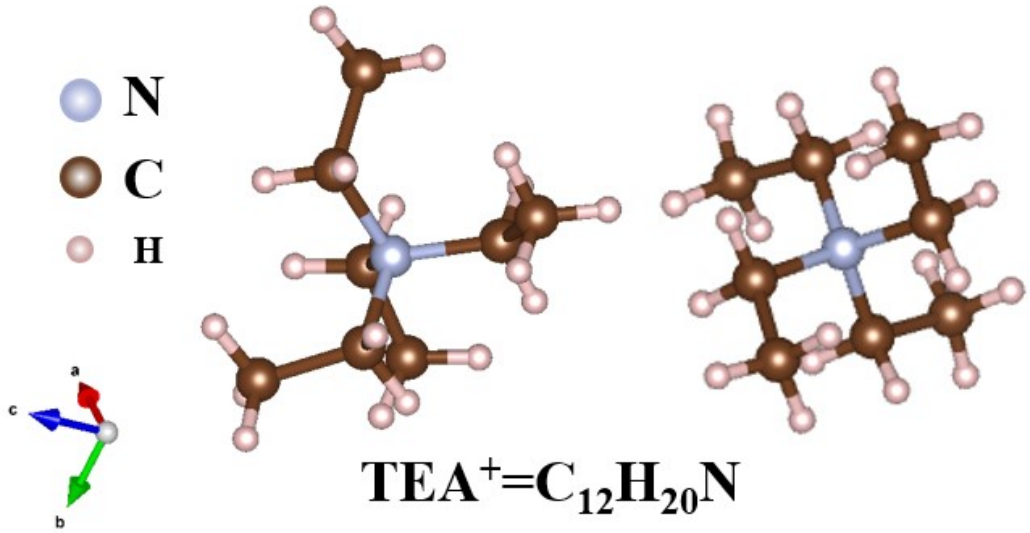

Figure. S1 The molecular structure of TEA^+

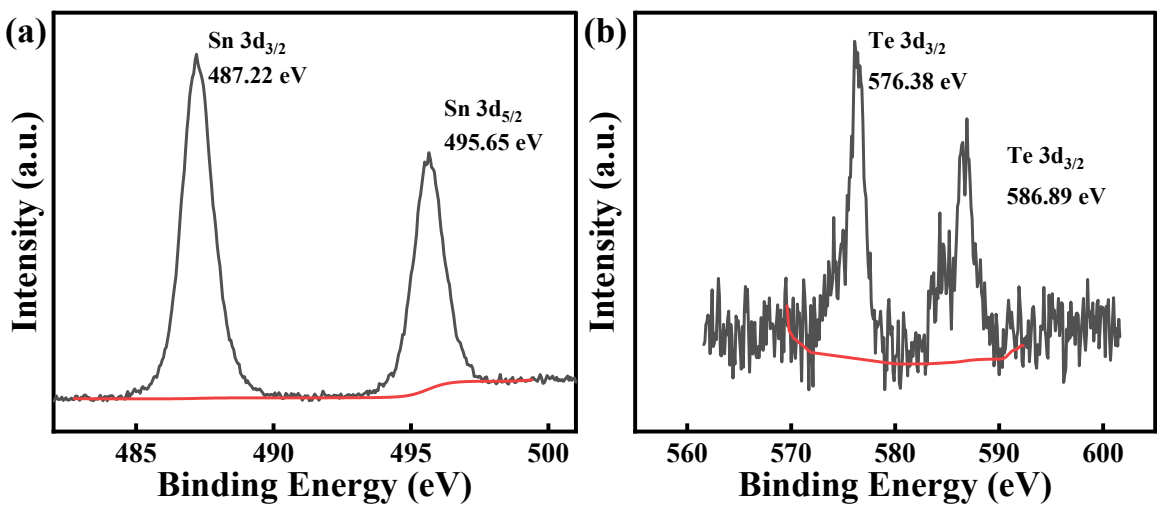

Figure. S2 (a) High-resolution XPS spectra of Sn 3d. (b) High-resolution XPS spectra of Te 3d.

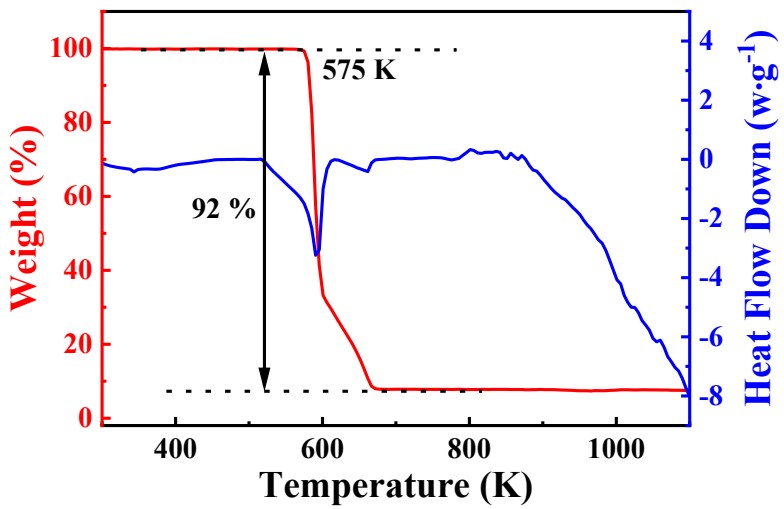

Figure. S3 DSC and TGA curves of $(TEA)_2SnCl_6$: 5%Te

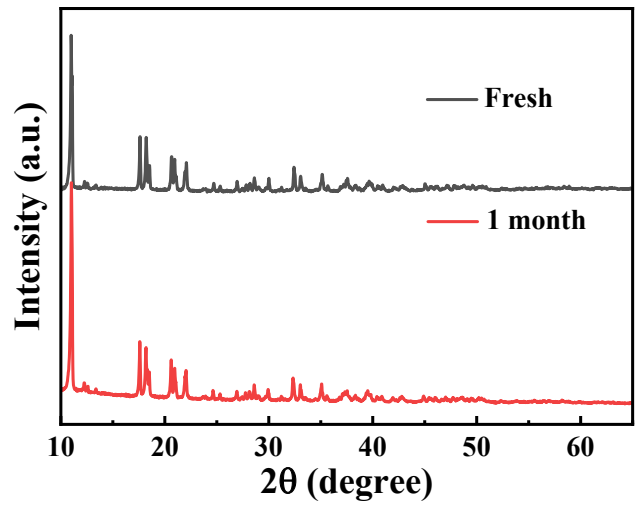

Figure. S4 PXRD patterns of air humidity degraded samples of $(TEA)_2SnCl_6$: 5%Te in air

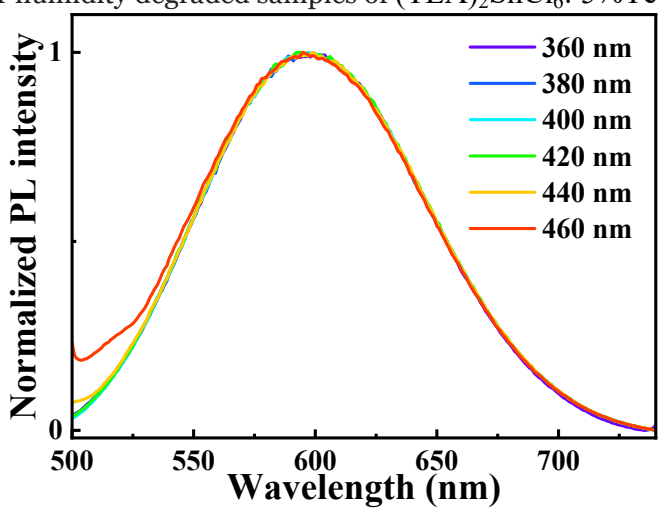

Figure. S5 PL spectra of $(TEA)_2SnCl_6$: 5%Te with different excitation wavelengths.

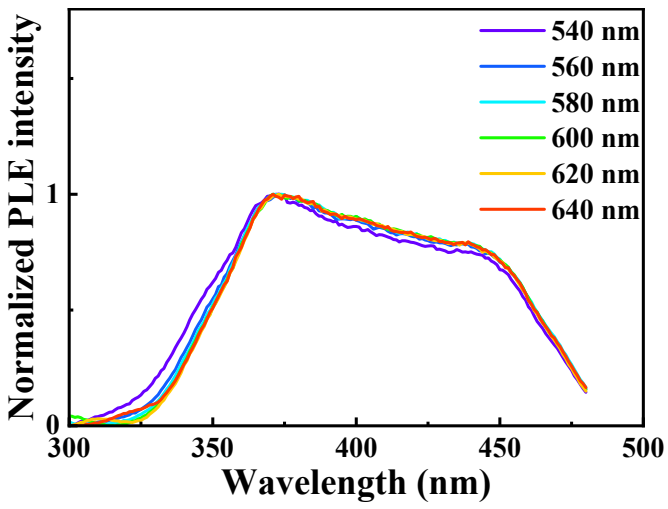

Figure. S6 PLE spectra of $(TEA)_2SnCl_6$: 5%Te under the different probe wavelengths.

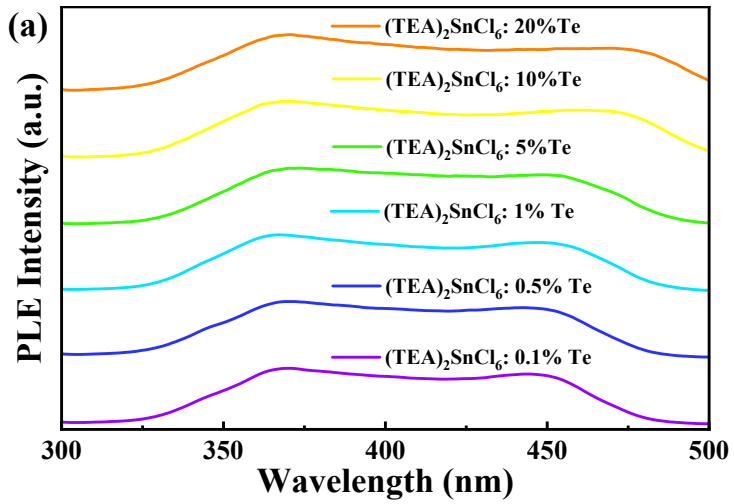

Figure. S7 PLE spectra of $(TEA)_2SnCl_6$: *x*%Te.

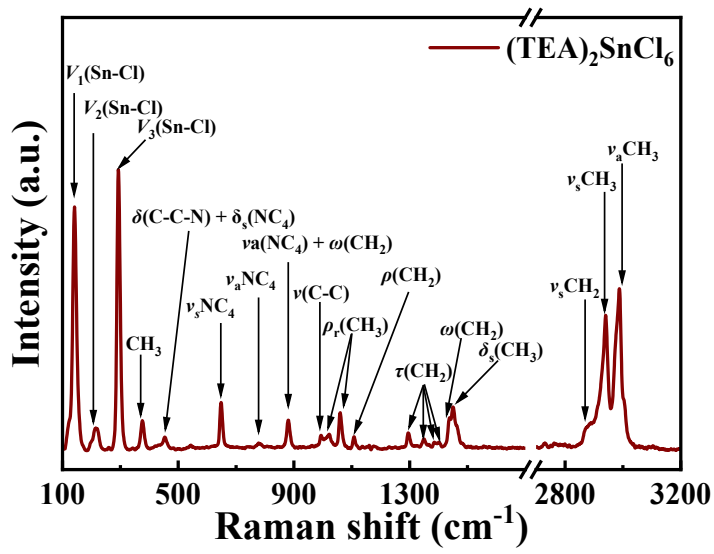

Figure. S8 Raman spectra of $(TEA)_2SnCl_6$ at room temperature.

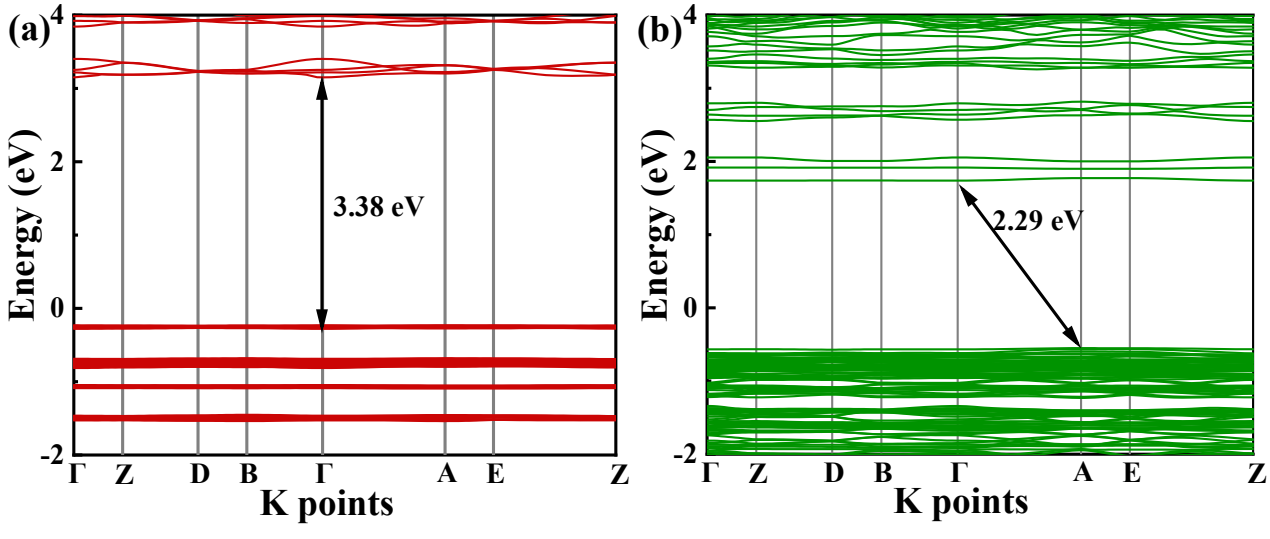

Figure. S9 (a) Band structures for $(TEA)_2SnCl_6$. (b) Band structures for $(TEA)_2SnCl_6$: 5%Te.

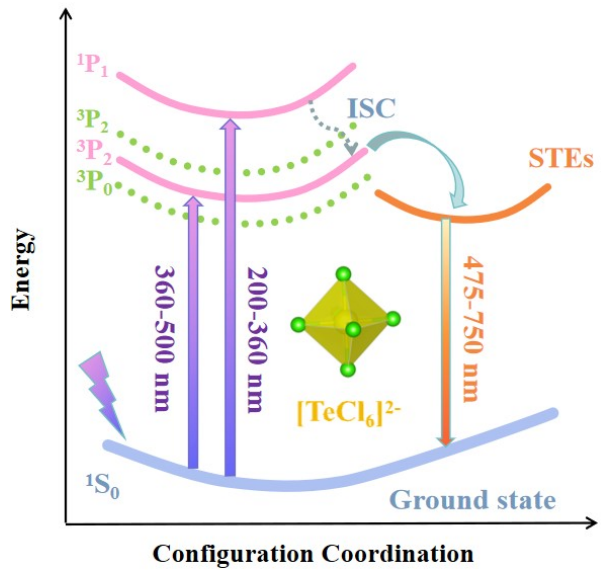

Figure. S10 Schematic diagram of the PL emission mechanism of Te doping $(TEA)_2SnCl_6$ MCs

References

(1) Kresse, G.; Furthmiiller, J. Efficiency of ab-initio total energy calculations for metals and semiconductors using a plane-wave basis set. *Comput. Mater. Sci* **1996**, *6*, 15-50.

(2) Peng, H.; Perdew, J. P. Rehabilitation of the Perdew-Burke-Ernzerhof generalized gradient approximation for layered materials. *Phys. Rev. B* **2017**, *95*, 081105-081110.

(3) Francisco, H. I.; Carmona-Espíndola, J.; Gázquez, J. L. Analysis of the kinetic energy functional in the generalized gradient approximation. *J. Chem. Phys* **2021**, *154*, 084107-084121.

(4) Tang, H.; Zhao, X.; Qin, Y.; Liu, S.; Zhang, H.; Li, H.; Liu, C.; Zhu, J. Unusual Tm^{3+} sensitization-induced white-emitting and thermostable improvement in $Ba_2Y_2Ge_4O_{13}:Dy^{3+}$ phosphor for solid-state lighting and optical thermometry. *Prog. Solid State Chem.* **2024**, *75*, 100477-100486.

(5) Jiang, H.; Song, J.; Hu, Q.; Su, Y.; Wen, Q.; Liu, L.; Zhu, J. Up/down-conversion luminescence and optical thermometry of Er^{3+}-activated bismuth tellurium borate. *J. Alloys Compd.* **2024**, *1005*, 176002-176012.

(6) Xiang, Y.; Yang, L.; Liao, C.; Xiang, X.; Tang, X.; Tang, H.; Zhu, J. Thermometric properties of $Na2Y_2TeB_2O_{10}:Tb_{3+}$ green phosphor based on fluorescence/excitation intensity ratio. *J. Mater. Chem. C.* **2022**, *12* (4), 848-860.

(7) Jun-Hua, W.; Jian-Bin, L.; Jin-Feng, L.; Wei-Tao, O.; Dai-Bin, K. Te^{4+}-doped $Cs_2InCl_5\cdot H_2O$ single crystals for remote optical thermometry. *Sci. China Mater.* **2021**, *65*, 764-772.

(8) Jin, Y.; Mei, L.; Su, K.; Guo, Q.; Liao, L. Color tunable warm white emitting whitlockite-type phosphor applied in optical thermometry. *J. Lumin.* **2022**, *254*, 119532-119543.

(9) C Lal, S.; I N, J.; Ganesanpotti, S. A six-mode optical thermometry rooted from the distinct thermal behavior of $SrLaLiTeO_6$: Mn^{4+}, Eu^{3+} double perovskites and their potential application in wavelength detection. *J SCI-ADV MATER DEV* **2023**, *8*, 100544-100559.

(10) Xu, J.; Bu, Y.; Wang, J.; Meng, L.; Wang, X.; Yan, X. Site-dependent photoluminescence and optical thermometric behaviors of double-perovskite $CaBa_2WO_6:Er^{3+}$. *Chem. Phys. Lett.* **2020**, *749*, 137410-137419.